Rock and Soil Mechanics

Volume 43 | Issue 11 Article 7

1-15-2023

Stability analysis of shield tunnel face considering spatial variability of hydraulic parameters

Shuai YUAN
Wuhu Surveying and Mapping Design Institute Co., Ltd., Wuhu, Anhui 241000, China

De-wang FENG
Zhejiang Supervision on Highway and Water Transportation Construction Engineering Co., Ltd, Hangzhou, Zhejiang 323000, China

Sen-hao ZHANG
School of Highway, Chang' an University, Xi' an, Shaanxi 710064, China

Yun-peng XING
School of Highway, Chang' an University, Xi' an, Shaanxi 710064, China

See next page for additional authors

Custom Citation

YUAN Shuai, FENG De-wang, ZHANG Sen-hao, XING Yun-peng, KE Zun-qi, . Stability analysis of shield tunnel face considering spatial variability of hydraulic parameters[J]. Rock and Soil Mechanics, 2022, 43(11): 3153-3162.

Stability analysis of shield tunnel face considering spatial variability of hydraulic parameters

Authors

Shuai YUAN, De-wang FENG, Sen-hao ZHANG, Yun-peng XING, and Zun-qi KE

Rock and Soil Mechanics 2022 43(11): 3153−3162 ISSN 1000−7598
https: //doi.org/10.16285/j.rsm.2021.7200 rocksoilmech.researchcommons.org/journal

Stability analysis of shield tunnel face considering spatial variability of hydraulic parameters

YUAN Shuai[1, 2], FENG De-wang[1, 3], ZHANG Sen-hao[1], XING Yun-peng[1], KE Zun-qi[1]

1. School of Highway, Chang' an University, Xi' an, Shaanxi 710064, China

2. Wuhu Surveying and Mapping Design Institute Co., Ltd., Wuhu, Anhui 241000, China

3. Zhejiang Supervision on Highway and Water Transportation Construction Engineering Co., Ltd, Hangzhou, Zhejiang 323000, China

Abstract: The shield method is commonly employed in the construction of urban subways, and the stability of the excavation surface is extremely important for the safety of tunnel construction. When constructing tunnels in submerged or water-rich strata, the seepage force is a key factor affecting the ultimate support force of excavation faces. Uncertainty of natural geotechnical material hydraulic parameters significantly impacts the seepage force near the face. Based on the classic limit analysis and the random field theory, the principle of effective stress in saturated soil is introduced, and the stochastic numerical limit analysis method considering the influence of pore water pressure is established by combining finite element spatial discretization and second-order cone programming. On this basis, the influence of spatial variability of permeability coefficient on the stability of shield tunnel face in water-rich strata is studied. The results show that the heterogeneity of the permeability coefficient leads to an increase in the pore pressure gradient at the face. The increase in the variation of permeability coefficient and the ratio of vertical to horizontal permeability coefficient significantly increases the support force required to maintain the face stability, and the effect of cross correlation coefficient and autocorrelation distance is relatively small. The present research can provide theoretical guidance for evaluating the face stability of tunnels in water-rich strata.

Keywords: tunnel engineering; face stability; spatial variability; seepage force; limit analysis

1 Inroduction

At present, urban subways are constructed mainly by the shield method. During the shield tunneling process, insufficient support force at the face will cause the surrounding soil to collapse, while excessive support force will cause the heave of upper soil, so the stability of the face is crucial to tunnel construction safety. In recent years, various methods, such as theoretical analysis, numerical simulation and model tests, are often used to study the stability of tunnel face. Theoretical analysis is based on the limit equilibrium method and limit analysis method. Janseen[1] proposed a silo theory analysis model and obtained an approximate solution for the slip surface. Horn[2] optimized the silo theory on the basis of Janseen's research and proposed a three-dimensional limit analysis model for face stability. Leca et al.[3] constructed a three-dimensional cone-shaped failure model for faces of sandy soil based on the upper bound method of plasticity analysis. Song et al.[4] studied the failure mode of the face based on the plane strain model and obtained the upper bound solution of ultimate support force based on multi-block cone-shaped failure mode, considering the spatial heterogeneity of geo-technical mass. Liang et al.[5] used the multi-block upper limit method and combined it with the log spiral failure mechanism to derive the calculation formula for the ultimate support force of the face in nonhomogeneous clay strata. The above studies have not considered the influence of groundwater seepage on the ultimate support force of tunnel faces. Lee et al.[6] proposed a formula for calculating the ultimate support force based on the three-dimensional failure model proposed by Leca, considering groundwater seepage. The calculation results showed that the effect of seepage force on the support force was much greater than the effective stress. Huang[7] studied the effect of groundwater seepage on the safety factor of shallow embedded tunnel faces based on the upper bound limit analysis theory. Mi et al.[8] investigated the effect of groundwater seepage flow on the support force and stratum instability model of shallowly embedded shield tunnel faces based on limit equilibrium theory with model tests and numerical simulations. Gao et al.[9] analyzed the stability of tunnel faces under the joint influence of finite support pressure and seepage force. Although the above studies have considered the effect of groundwater seepage on the stability of tunnel faces, the soil hydraulic parameters were considered uniformly isotropic and the unfavorable effect of spatial variability of hydraulic parameters was not involved.

Natural soils are affected by deposition and loading history, and their parameters exhibit spatial variability. It is necessary to consider the uncertainty of soil parameters in the face stability analysis. Mollon et al.[10] considered the soil strength parameters as random variables and applied the response surface method and random response surface method to analyze the influence of soil parameter uncertainty on the face stability. Li et al.[11] used the BP neural network to establish an implicit relationship between soil parameters and the ultimate support force of the face, and discussed the

Received: 29 December 2021 Revised: 13 July 2022
This work was supported by the National Natural Science Foundation of China (51908053) and the Fundamental Research Funds for the Central Universities (300102210209).
First author: YUAN Shuai, male, born in 1984, PhD, Associate Professor, resarch interests: geotechnical engineering calculation. E-mail: yuan_shuai@126.com

calculation principle of the earth pressure for the face in shield construction based on the reliability theory. Sun[12] studied the relationship between the support pressure of the slurry shield tunnel face and the reliability index by using the Monte Carlo method. Mollon et al.[13] proposed a failure mechanism for tunnel faces that could consider the spatial variability of soil strength parameters under two-dimensional conditions, and the effectiveness of the method was verified by numerical calculation results. Eshraghi et al.[14] studied the effect of uncertainty of layered soil parameters on the face stability based on the Monte Carlo method.

However, studies on the influence of the spatial variability of soil hydraulic parameters are very limited. For shield tunnels in water-rich strata, the non-homogeneity of the permeability coefficient has a great impact on the seepage field around the tunnel face, leading to a high local head gradient and greatly reducing the face stability. To tackle the above problems, based on limit analysis and random field theory, this paper introduces the principle of effective stress for saturated soils, combines second-order cone programming and finite element methods, and establishes a stochastic numerical limit analysis method that considers the influence of pore water pressure. On this basis, the effects of the coefficient of variation of saturated permeability coefficient, autocorrelation distance, cross correlation coefficient, and vertical and horizontal permeability coefficient ratio on the face stability are studied to provide important theoretical guidance for the safe construction of shield tunnels.

2 Random field discretization

Soil hydraulic parameters exhibit obvious spatial variability. To analyze the effect of seepage forces separately, the soil strength parameters are assumed to be uniformly-distributed deterministic values, and only the saturated permeability coefficients of the soil are regarded as anisotropic random fields, the cross correlation of the horizontal and vertical permeability coefficients is considered. It is assumed that the soil permeability coefficient is orthogonally anisotropic, the permeability coefficients in the horizontal and vertical directions are k_x and k_y, respectively. Considering the non-negativity of the permeability coefficient, it is assumed that the permeability coefficient obeys a lognormal distribution with reference to the literature[15].

For the stochastic limit analysis method considering the spatial variability of hydraulic parameters, it is first necessary to discretize the hydraulic parameter in the solution domain spatially. In this paper, the Karhunen-Loeve series expansion method is used, and the hydraulic parameter random field can be expressed as

$$\hat{H}_{\ln X_i}(x,y,\theta)=\mu_{\ln X_i}+\sum_{j=1}^{n}\sigma_{\ln X_i}\sqrt{\lambda_j}\,f_j(x,y)\boldsymbol{\xi}_{i,j}(\theta),\quad (x,y)\in\Omega,\quad (X_i=k_x,k_y) \tag{1}$$

where θ is the random event, (x,y) is the coordinate of any point in the computational domain Ω, X_i is the research variable, $\mu_{\ln X_i}$ is the mean of the logarithmic random field, $\sigma_{\ln X_i}$ is the standard deviation of the logarithmic random field, λ_j and $f_j(x,y)$ are respectively the eigenvalue and eigenfunction of the autocorrelation function, and n is the number of the truncated item. In order to improve the computational efficiency, Phoon et al.[16] proposed that the first n terms of the expansion can be truncated for analysis under the premise of ensuring the computational accuracy, so that the first n terms are accumulated in the equation. According to the analysis results of Laloy, the first 226 terms are taken in this paper[17]. $\boldsymbol{\xi}_{i,j}$ is the independent standard normal random vector and is generated by Latin hypercube sampling in this paper. The mean and standard deviation of the logarithmic random field can be calculated by the following equations:

$$\left.\begin{aligned}\mu_{\ln X_i}&=\ln\mu_{X_i}-\frac{\sigma^2_{\ln X_i}}{2}\\ \sigma_{\ln X_i}&=\sqrt{\ln\left[1+\left(\frac{\sigma_{X_i}}{\mu_{X_i}}\right)^2\right]}\end{aligned}\right\} \tag{2}$$

where μ_{X_i} is the mean of the random field, and σ_{X_i} is the standard deviation of the random field. For the sake of simplification, the exponential autocorrelation function is used to describe the spatial correlation of the permeability coefficient:

$$\rho\left[(x_1,y_1)\quad(x_2,y_2)\right]=\exp\left(-\frac{|x_1-x_2|}{\delta_{\mathrm{h}}}\right)\exp\left(-\frac{|y_1-y_2|}{\delta_{\mathrm{v}}}\right) \tag{3}$$

where ρ is the cross correlation coefficient, and δ_{h} and δ_{v} are the horizontal and vertical autocorrelation distances, respectively. Large autocorrelation distances imply small spatial variability and high soil homogeneity; conversely, small autocorrelation distances indicate a large spatial variability[18–19].

The independent Gaussian random field is generated using the above method, and the horizontal and vertical permeability coefficients of the soil are generally correlated, and they can be described by the correlation coefficient matrix $\boldsymbol{R}=(\rho_{ij}),\ i,j=k_x,k_y$. For the correlated permeability coefficient random fields, the Nataf transformation method[20–21] can be used to transform the independent Gaussian random fields into correlated Gaussian random fields:

$$\bar{H}_{\ln X_i}(x,y,\theta)=\boldsymbol{L}\hat{H}_{\ln X_i}(x,y,\theta) \tag{4}$$

where $\boldsymbol{L}$ is the lower triangular matrix of the correlation coefficient matrix.

Finally, the random field of permeability coefficient can be obtained by equal probability transformation:

$$H_{X_i}(x,y,\theta)=\exp\left[\bar{H}_{\ln X_i}(x,y,\theta)\right] \tag{5}$$

Detailed discretization process can refer to relevant literature[20–21].

3 Numerical limit analysis

A rigid ideal plastic body Ω is assumed to be subjected to the combined action of a body force $\lambda \boldsymbol{g}$ and a surface force $\lambda \boldsymbol{T}$, where $\boldsymbol{g}$ and $\boldsymbol{T}$ are the load distributions given in advance, and λ is the load multiplier to be optimized. The mathematical programming form of the upper bound analysis theorem takes the form

$$\begin{aligned} &\max \text{ imize } \quad \lambda \\ &\text{s.t.} \quad \int_{\Omega} \delta \dot{\boldsymbol{\varepsilon}}^{\mathrm{T}} \boldsymbol{\sigma} \mathrm{d}V = \lambda \left(\int_{\Omega} \delta \dot{\boldsymbol{u}}^{\mathrm{T}} \boldsymbol{g} \mathrm{d}V + \int_{\Gamma_{\mathrm{s}}} \delta \dot{\boldsymbol{u}}^{\mathrm{T}} \boldsymbol{T} \mathrm{d}S \right) \\ &\quad\quad f(\boldsymbol{\sigma}) \leqslant 0 \end{aligned} \tag{6}$$

where $\boldsymbol{\sigma}$ is the total stress, $\dot{\boldsymbol{\varepsilon}}$ is the strain rate, $\dot{\boldsymbol{u}}$ is the velocity vector, dV and dS are respectively the volume increment and surface area increment in the solution domain, $f(\boldsymbol{\sigma})$ is the yield function, the stress and strain in this paper are positive in tension, and Γ_{s} is the load boundary. The effective stress for saturated soil is introduced:

$$\boldsymbol{\sigma}' = \boldsymbol{\sigma} + u_{\mathrm{w}} \boldsymbol{I} \tag{7}$$

where $\boldsymbol{\sigma}'$ is the effective stress, u_{w} is the pore water pressure, and $\boldsymbol{I}$ is the second order unit matrix. After substituting Eq. (7) into Eq. (6), we get

$$\begin{aligned} &\max \text{ imize } \quad \lambda \\ &\text{s.t.} \quad \int_{\Omega} \delta \dot{\boldsymbol{\varepsilon}}^{\mathrm{T}} \boldsymbol{\sigma} \mathrm{d}V = \lambda \left(\int_{\Omega} \delta \dot{\boldsymbol{u}}^{\mathrm{T}} \boldsymbol{g} \mathrm{d}V + \int_{\Gamma_{\mathrm{s}}} \delta \dot{\boldsymbol{u}}^{\mathrm{T}} \boldsymbol{T} \mathrm{d}S \right) + \\ &\quad\quad \int_{\Omega} \delta \dot{\boldsymbol{\varepsilon}}_{\mathrm{v}} u_{\mathrm{w}} \mathrm{d}V \\ &\quad\quad f(\boldsymbol{\sigma}') \leqslant 0 \end{aligned} \tag{8}$$

Equation (8) is the mathematical programming of the upper bound analysis of saturated soil considering the pore water pressure condition.

The solution domain is discretized using the finite element shown in Fig. 1, with the triangle corner points being taken for pore water pressure node and stress node and the velocity node being triangular corner points and the midpoint of each side. The pore water pressure is obtained by seepage calculation, and then the external power is calculated as a given value. The velocity field in the element can be expressed by the element velocity vector $\boldsymbol{d}^{\mathrm{e}}$ as

$$\dot{\boldsymbol{u}} = [\dot{u} \quad \dot{v}]^{\mathrm{T}} = \boldsymbol{N}^{\mathrm{u}} \boldsymbol{d}^{\mathrm{e}} \tag{9}$$

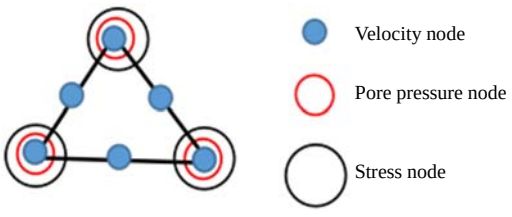

Fig. 1 Finite element for upper bound analysis

where $\dot{u}$ and $\dot{v}$ are the velocity components, and $\boldsymbol{N}^{\mathrm{u}}$ is the coefficient matrix composed of velocity shape functions. The strain rate in the element is

$$\dot{\boldsymbol{\varepsilon}} = \sum_{i=1}^{3} L_i \dot{\boldsymbol{\varepsilon}}_i = \boldsymbol{N}^{\varepsilon} \dot{\boldsymbol{\varepsilon}}^{\mathrm{e}} \tag{10}$$

where L_i is the area coordinate, $\boldsymbol{N}^{\varepsilon}$ is the coefficient matrix composed of stress shape functions, and $\dot{\boldsymbol{\varepsilon}}^{\mathrm{e}}$ is the element strain rate vector. The effective stress in the element is

$$\boldsymbol{\sigma}' = \sum_{i=1}^{3} L_i \boldsymbol{\sigma}_i' = \boldsymbol{N}^{\sigma} \boldsymbol{\sigma}'^{\mathrm{e}} \tag{11}$$

where $\boldsymbol{N}^{\sigma}$ is the coefficient matrix composed of stress shape functions, and $\boldsymbol{\sigma}'^{\mathrm{e}}$ is the effective stress vector of the element. The strain rate in the element $\dot{\boldsymbol{\varepsilon}}$ can also be expressed as

$$\dot{\boldsymbol{\varepsilon}} = L \boldsymbol{N}^{\mathrm{u}} \boldsymbol{d}^{\mathrm{e}} = \boldsymbol{B} \boldsymbol{d}^{\mathrm{e}} \tag{12}$$

where $\boldsymbol{B}$ is the strain matrix, and L is differential operator related to strainrate and velocity. Substituting Eqs.(9)–(12) into Eq. (8), the mathematical programming problem can be expressed as

$$\begin{aligned} &\max \text{ imize } \quad \lambda \\ &\text{s.t.} \quad \sum_{e=1}^{N_{\mathrm{e}}} \delta \dot{\boldsymbol{d}}^{\mathrm{e}\mathrm{T}} \left(\int_{\Omega^e} \boldsymbol{B}^{\mathrm{T}} \boldsymbol{N}^{\sigma} \mathrm{d}V \right) \boldsymbol{\sigma}'^{\mathrm{e}} = \\ &\quad\quad \lambda \left[\sum_{e=1}^{N_{\mathrm{e}}} \delta \dot{\boldsymbol{d}}^{\mathrm{e}\mathrm{T}} \left(\int_{\Omega^e} \boldsymbol{N}^{\mathrm{u}\mathrm{T}} \boldsymbol{g} \mathrm{d}V \right) + \sum_{m=1}^{N_{\mathrm{m}}} \delta \dot{\boldsymbol{d}}^{\mathrm{e}\mathrm{T}} \left(\int_{\Gamma_{\mathrm{sm}}} \boldsymbol{N}^{\mathrm{u}\mathrm{T}} \boldsymbol{T} \mathrm{d}S \right) \right] - \\ &\quad\quad \sum_{e=1}^{N_{\mathrm{e}}} \delta \dot{\boldsymbol{d}}^{\mathrm{e}\mathrm{T}} \left(\int_{\Omega^e} \boldsymbol{B}_{\mathrm{m}}^{\mathrm{T}} u_{\mathrm{w}} \mathrm{d}V \right) \\ &\quad\quad f(\boldsymbol{\sigma}_i') \leqslant 0 \quad\quad i = 1, 2, \cdots 3N_{\mathrm{e}} \end{aligned} \tag{13}$$

where N_{e} is the number of elements, N_{m} is the number of surface force element boundaries, $\boldsymbol{B}_{\mathrm{m}}^{\mathrm{T}}$ is the volumetric strain matrix, and Γ_{sm} is the element load boundary. Eq. (13) can be simplified as

$$\begin{aligned} &\max \text{ imize } \quad \lambda \\ &\text{s.t.} \quad A \boldsymbol{\sigma}'^{\mathrm{g}} = \lambda \boldsymbol{q} + \boldsymbol{q}_0 - \boldsymbol{q}_{\mathrm{w}} \\ &\quad\quad f(\boldsymbol{\sigma}_i') \leqslant 0 \quad\quad i = 1, 2 \cdots 3N_{\mathrm{e}} \end{aligned} \tag{14}$$

where $\boldsymbol{\sigma}'^{\mathrm{g}}$ is the overall effective stress vector, $\boldsymbol{q}$ is the overall unknown force vector, $\boldsymbol{q}_0$ is the overall known force vector, and $\boldsymbol{q}_{\mathrm{w}}$ is the equivalent load vector of the pore water pressure.

It is assumed that the soil obeys the Mohr-Coulomb yield criterion, the yield function can be expressed as

$$\tau_{\mathrm{f}} = c' - \sigma_{\mathrm{n}}' \tan \varphi' \tag{15}$$

where τ_{f} and σ_{n}' are the tangent of the failure plane and normal effective stress, and c' and φ' are the effective cohesion and internal friction angle. Introduce the modified effective stress vector:

$$\begin{aligned} &\boldsymbol{s}' = \left[\sigma_{\mathrm{m}}' \quad s_{xx} \quad s_{xy} \right]^{\mathrm{T}} \\ &\sigma_{\mathrm{m}}' = \frac{1}{2} \left(\sigma_{xx}' + \sigma_{yy}' \right), \quad s_{ij} = \sigma_{ij}' - \sigma_{\mathrm{m}}' \delta_{ij} \end{aligned} \tag{16}$$

where σ'_{m} is the mean effective stress, σ'_{xx} and σ'_{yy} are the effective stress components, s_{ij} is the deviatoric stress, and δ is the Kronecker symbol. For the plane strain condition, the yield criterion can be rewritten as

$$\sqrt{s_{xx}^2+s_{xy}^2}+\sigma'_{\mathrm{m}}\sin\varphi'-c'\cos\varphi'\leqslant 0 \tag{17}$$

By introducing an auxiliary variable z, the Mohr-Coulomb yield criterion can be rewritten as a linear equality constraint and a second order cone constraint[22–23]:

$$\begin{aligned} &z+a\sigma'_{\mathrm{m}}=b\\ &\sqrt{s_{xx}^2+s_{xy}^2}\leqslant z \end{aligned} \tag{18}$$

where $a=\sin\varphi'$ and $b=c'\cos\varphi'$. The final discretization form of the upper bound analysis for saturated soil is obtained as

$$\begin{aligned} &\text{max imize}\quad \lambda\\ &\text{s.t.}\quad A\boldsymbol{s}'^{\mathrm{g}}=\lambda\boldsymbol{q}+\boldsymbol{q}_0-\boldsymbol{q}_{\mathrm{w}}\\ &\qquad z_i+a_i\sigma_{\mathrm{m},i}=b_i\\ &\qquad \sqrt{s_{xx,i}^2+s_{xy,i}}\leqslant z_i\qquad i=1,2\cdots 3N_{\mathrm{e}} \end{aligned} \tag{19}$$

where $\boldsymbol{s}'^{\mathrm{g}}$ is the overall modified effective stress vector.

4 Algorithm implementation for random limit analysis method

Based on the Monte Carlo method, multiple sets of random field samples of permeability coefficients are generated, and the pore water pressure distribution is obtained after carrying out seepage calculations. Then the MATLAB toolbox of MOSEK software is used to solve the mathematical programming problem presented in Eq. (19), and the stochastic limit analysis method is calculated as follows (as shown in Fig. 2).

(1) Random field discretization. Assuming that the soil hydraulic parameters obey logarithmic normal distribution, independent standard normal random vectors are generated by Latin hypercube sampling and independent Gaussian random fields are generated based on Karhunen-Loeve expansion method. The relevant non-Gaussian random fields are obtained by combining the Nataf transform and the equal probability transform, and the soil parameters in the element are determined based on the element centroid coordinates.

(2) Seepage field analysis. The postprocessing script is written with Python code. The finite element analysis software ABAQUS is developed, and the MATLAB programming is used to make the three interact effectively to complete the seepage field analysis of the tunnel excavation model automatically.

(3) Numerical limit analysis. The corner points of the element and the midpoints of each side are used as velocity nodes, and the triangular corner points are used as effective stress nodes. The external power is calculated from the pore water pressure at the corner points obtained from the seepage analysis, the internal dissipation is calculated from the effective stress, and the mathematical programming problem is solved by the MATLAB optimization toolbox of MOSEK.

(4) Result viewing. The solved ultimate support force is further developed to obtain the statistical information such as the mean and the standard deviation. The information such as node displacement is post-processed using the GID software to obtain the failure mechanism of the face.

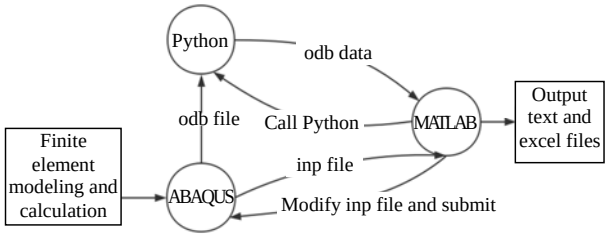

Fig. 2 Interactive mechanism of MATLAB, ABAQUS and Python

5 Calculation model

The calculation model of the shield tunnel face is shown in Fig. 3. For simplicity, the plane strain condition is considered. The excavation diameter is $D=6$ m, the embedment depth is $C=15$ m, the ground surface is a horizontal plane with an overlying water layer, the thickness of the water layer is $H_{\mathrm{w}}=5$ m, the support force of the tunnel face is P_{s}, P_{s} is assumed to be a uniform distribution. It should be noted that the support force is generally not uniformly distributed, and the assumption of uniform distribution has some deviation from the actual situation, but the calculation error decreases with the decrease of shield diameter. The shield diameter is 6 m in this paper, large section shield is not considered, thus the error is small. The calculated results in the paper can be considered as an approximation of the mean support force at the face. The finite element mesh used in the calculation is shown in Fig. 3(b), with a total of 3438 elements and 7 073 nodes. In order to improve the calculation efficiency, the soil elements adjacent to the face are appropriately refined.

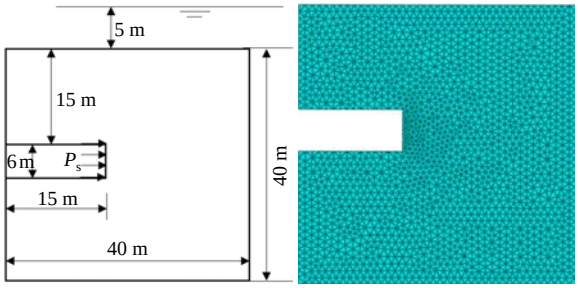

(a) Calculation model of the shield tunnel face (b) Finite element mesh configuration

Fig. 3 Calculation model of the shield tunnel face and the finite element mesh configuration

For the seepage analysis, it is assumed that the boundary of the tunnel face is fully drained, the pore water pressure is 0, the ground surface is the pore pressure boundary, the water table height is achieved by

setting the surface pore water pressure, and all other boundaries are impermeable boundaries. It is assumed that the seepage has reached stability during the tunnel excavation, and the calculation is based on the steady-state seepage control equation. For the numerical limit analysis, the left and right side displacements and the bottom displacements of the model are constrained, the top of the model is a free boundary, the normal displacement of the tunnel lining position is constrained while the tangential direction is set as free. The active failure ultimate support force of the face is obtained by numerical limit analysis.

The physical and mechanical parameters of the surrounding soil are shown in Table 1, all of which are deterministic values. The random field parameters of the permeability coefficient of tunnel surrounding soil under different conditions are shown in Tables 2 and 3. Four cases are considered. In the first two cases (see Table 2), the horizontal and vertical permeability coefficients are equal, i.e., the permeability coefficient at any point is isotropic; in the last two cases (see Table 3), the horizontal and vertical permeability coefficients are not equal, and the permeability coefficient at any point is assumed to be orthogonally anisotropic. The effects of the coefficient of variation and the autocorrelation distance on the pore water pressure field of the tunnel surrounding soil and its the stability are studied in case 1 and case 2, respectively. Since the soil permeability coefficient is generally anisotropic, the horizontal permeability coefficient is significantly different from the vertical permeability coefficient, therefore, the influence of the cross correlation of horizontal and vertical permeability coefficients and the permeability coefficient ratio on the calculated results are studied in the two cases in Table 3.

Table 1 Physical and mechanical parameters of surrounding soil

Unit weight /(kN • m^{-3})	Elastic modulus /MPa	Poisson's ratio	Cohesion /kPa	Friction angle /(°)
20	100	0.3	5	25

Table 2 Parameters of random field (isotropic permeability)

Case	Mean /(m • s^{-1})	Computational domain a_x /m	Computational domain a_y /m	Horizontal autocorrelation distance /m	Vertical autocorrelation distance /m	Coefficient of variation
1	10^{-5}	20	20	10	2	0, 0.1,0.5,1
				2	2	
				10	2	
2	10^{-5}	20	20	30	2	1
				30	10	
				30	30	

Table 3 Parameters of random field (orthotropic permeability)

Case	Mean k_x /(m • s^{-1})	Computational domain $a_x \times a_y$ /m^2	Horizontal autocorrelation distance /m	Vertical autocorrelation distance /m	Coefficient of variation	k_y/k_x	Cross correlation coefficient
3	10^{-5}	20×20	30	30	1	2.0	0.1, 0.4, 0.8
4	10^{-5}	20×20	30	30	1	0.5, 1.0, 2.0, 5.0	0.8

6 Parametric analysis

6.1 Coefficient of variation

The coefficient of variation (COV) is an important indicator describing the degree of dispersion of the permeability coefficient[24] and is defined as $\mathrm{COV} = \sigma / \mu$, i.e., the ratio of the standard deviation to the mean. The larger the coefficient of variation is, the greater the dispersion degree of the random field will be. Comparing the coefficient of variation can eliminate the influence of two data sets due to the large difference in measurement scales and can also reflect the variability of different data intuitively.

Figure 4 shows the pore water pressure distribution adjacent to the face under different coefficients of variation. From the figure, it can be seen that, with the increase of the coefficient of variation, the range of the seepage field affected by tunnel excavation also gradually expands and the pore water pressure field near the face changes drastically, which means that the permeability component in the face support force increases gradually. Therefore, the stability analysis of shield tunnel faces needs to consider the uncertainty of the permeability coefficient.

The effect of the coefficient of variation on the seepage velocity of the face is shown in Fig.5, and the horizontal coordinates correspond to the vertical position of the face from top to bottom, with 0 m representing the top of the face and 6 m representing the bottom of the face. From the figure, it can be seen that the seepage velocity at the face tends to decrease gradually as the coefficient of variation increases. It is due to the fact that the change in soil permeability coefficient becomes more obvious when the coefficient of variation increases, hindering the pore water flow. The change of seepage velocity at the face indicates the variation of the permeability component in the face support force.

The influence of the coefficient of variation on the ultimate support force of the shield tunnel face is shown in Fig. 6. The 95% confidence intervals of the ultimate support force and the amplification coefficient are given, in which the amplification coefficient is defined as the ratio between the upper bound of the confidence interval and the corresponding deterministic result[18] and the

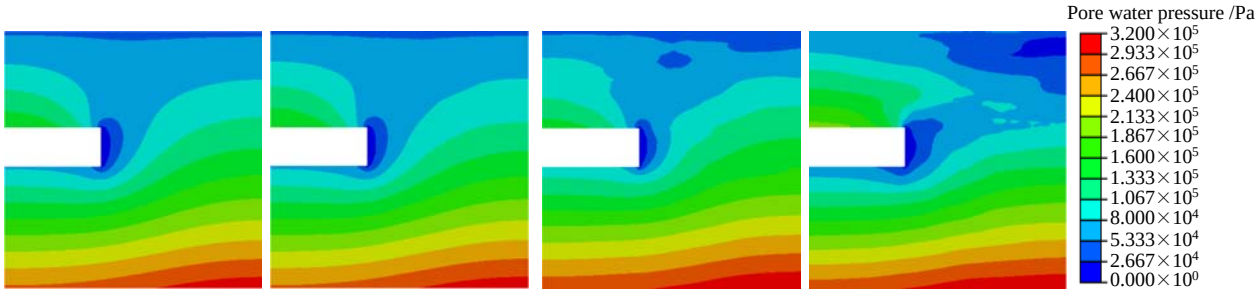

(a) COV=0 (b) COV=0.1 (c) COV=0.5 (d) COV=1.0

Fig. 4 Effect of coefficient of variation on the pore water pressure of surrounding soil

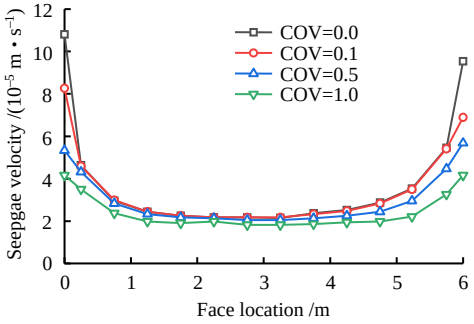

Fig. 5 Effect of coefficient of variation on the seepage velocity at the face

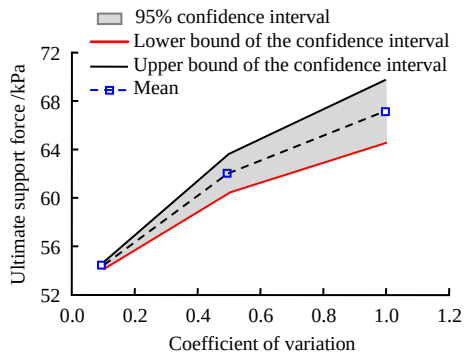

(a) Variation of ultimate support force with variation coefficient

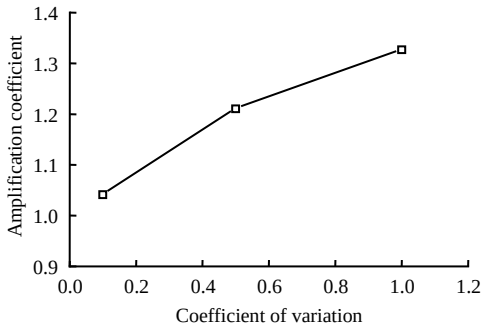

(b) Variation of amplification coefficient with variation coefficient

Fig. 6 Effect of coefficient of variation on the ultimate support force

amplification coefficient can effectively reflect the influence of the spatial variability of soil parameters on the face stability. As can be seen from the figure, with the increase of the coefficient of variation, the ultimate support force of the face gradually increases, and its dispersion and amplification coefficient also increase. This indicates that the spatial variability of the permeability coefficient increases the seepage force of the face and reduces the face stability. The adverse effects caused by the nonhomogeneity of the permeability coefficient need to be considered in the engineering design.

Figure 7 compares the face failure mode under different coefficients of variation. The color of the contour indicates the magnitude of the soil velocity vector modulus. Since the absolute magnitude of velocity is of no practical significance in the limit analysis and its relative magnitude can reflect the mode of failure, the legend is generally not given in the contour of the results for the limit analysis method[25]. From the figure, all the failure modes are similar. Local failure occurs in front of the face and the soil arching effect appears. The rear soil is loosened and the soil pressure is reduced. Part of the soil can still remain stable due to the soil arching effect[26–27]. With the increase of the coefficient of variation, the failure range in the horizontal direction gradually decreases, and the failure range in the vertical direction changes slightly. The reason for this is that when considering the spatial variability, a small horizontal autocorrelation distance brings out great dispersion, which makes the horizontal permeability increase and change sharply near the face, leading to a reduction in the horizontal range of the failure area.

6.2 Autocorrelation distance

Natural soil parameters at different positions have a certain correlation. When the distance between two points is large, the correlation is small, and vice versa. Soil autocorrelation distance is then a computational parameter describing this critical distance, which has a great impact on the accuracy of random field dispersion, and the theoretical autocorrelation function is usually used to describe the spatial correlation of soil parameters[28–29]. The exponential autocorrelation function is simple in form, highly accurate, and easy to calculate, and it has empirical solutions combined with K-L series expansion, so it is commonly used to simulate the spatial autocorrelation of geotechnical parameters.

The spatial correlation of soil parameters is strong when the autocorrelation distance is large, showing that it fluctuates fairly smoothly around its mean. On the contrary, a small autocorrelation distance corresponds to strong variability, thus the physical parameters show a sharp fluctuation around the mean. The seepage and numerical limit analysis are conducted under different

autocorrelation distances, the parameters used are shown in case 2 in Table 2.

The realization of permeability coefficient random fields under different autocorrelation distances is shown in Fig. 8. It can be seen that when the vertical autocorrelation distance is the same, the fluctuation of the permeability coefficient in the horizontal direction gradually decreases with the increase of the horizontal autocorrelation distance, and the horizontal stratification of the permeability coefficient is obvious, indicating the stratification of the soil; when the horizontal autocorrelation distance is the same, the fluctuation of the permeability coefficient gradually decreases along the vertical direction as the vertical autocorrelation distance increases. In practice, natural soil is stratified in the process of consolidation. Therefore, the soil horizontal autocorrelation distance tends to be much larger than the vertical autocorrelation distance.

The influence of autocorrelation distance on the ultimate support force of the shield tunnel face is shown in Figs. 9 and 10. It can be seen from the figure that with the increase of the horizontal autocorrelation distance, the amplification coefficient of the ultimate support force of the face gradually decreases. On the contrary, the amplification coefficient increases with the increase of vertical autocorrelation distance. The dispersion of the calculated limit supporting force varies little with the autocorrelation distance. The reason is that the decrease of horizontal autocorrelation distance leads to an increase in horizontal pore pressure fluctuation, the horizontal permeability, and a decrease in face stability. In the vertical direction, the rise in the dispersion of the permeability coefficient makes it difficult for the pore pressure at the tunnel top to affect the tunnel face, leading to a decrease in the ultimate support force required to maintain the stability of the face.

6.3 Cross correlation coefficient

The anisotropy of the permeability coefficient has been widely confirmed, however, there are very limited studies on the stability of shield tunnel faces under the condition of anisotropy of permeability coefficient[30], especially considering the spatial variability of permeability coefficient and anisotropy simultaneously. In this section, it is assumed that the soil permeability coefficient is orthogonal anisotropy, and the permeability coefficient in the horizontal direction is k_x, the permeability coefficient in the vertical direction is k_y. The permeability coefficients in the horizontal and vertical directions at the same location are generally positively correlated. The larger the cross correlation coefficient is, the more obvious the positive correlation trend of the permeability coefficient will be. When the cross correlation coefficient is 1, the ratio of k_x and k_y of each location in the soil remains the same. The parameters used is shown in case 3 in Table 3.

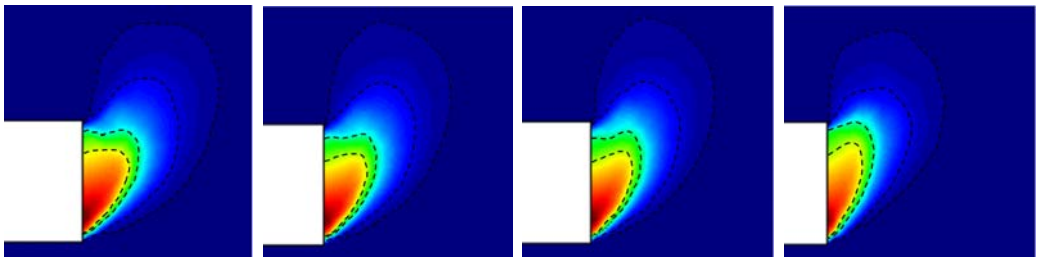

(a) COV =0 (b) COV =0.1 (c) COV =0.5 (d) COV =1.0

Fig. 7 Failure modes of face corresponding to different coefficients of variation

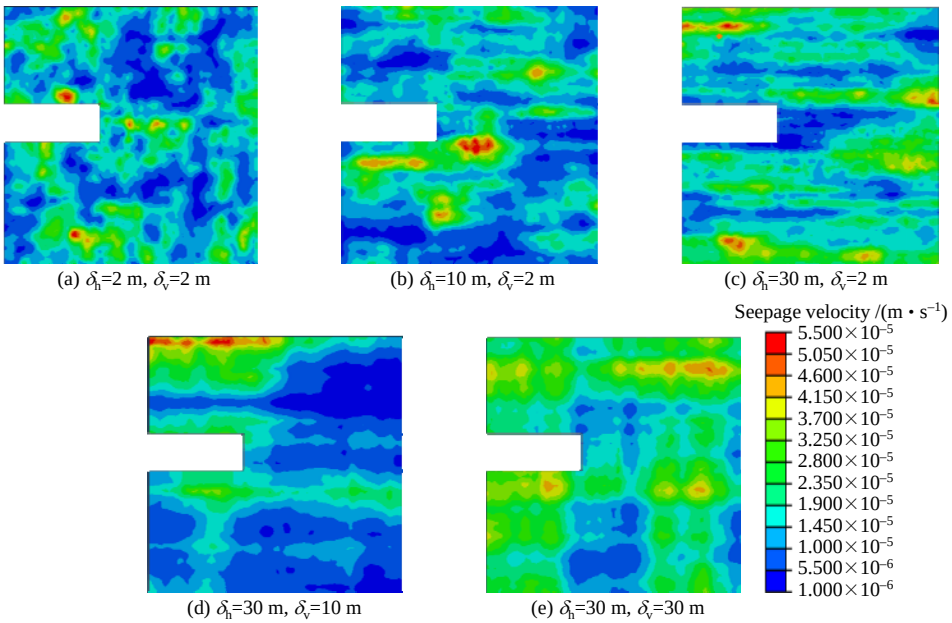

(a) δ_h=2 m, δ_v=2 m (b) δ_h=10 m, δ_v=2 m (c) δ_h=30 m, δ_v=2 m

(d) δ_h=30 m, δ_v=10 m (e) δ_h=30 m, δ_v=30 m

Fig. 8 Effect of autocorrelation distance on the random field of permeability coefficient

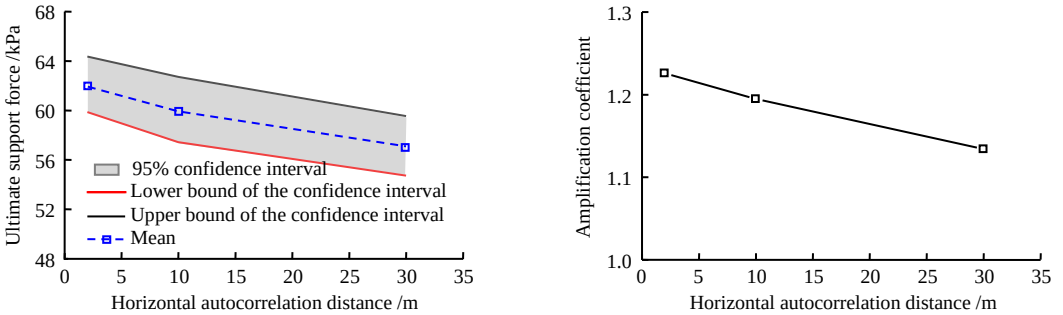

(a) Variation of ultimate support force with horizontal autocorrelation distance

(b) Variation of amplification coefficient with horizontal autocorrelation distance

Fig. 9 Effect of horizontal autocorrelation distance on the face ultimate support force

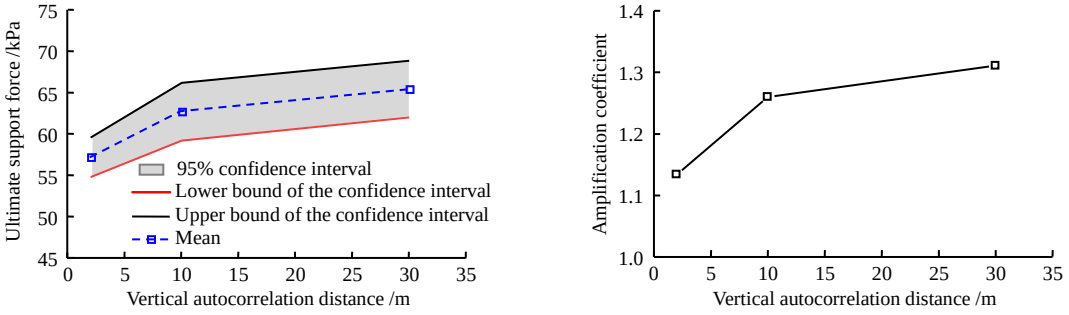

(a) Variation of ultimate support force with vertical autocorrelation distance

(b) Variation of amplification coefficient with vertical autocorrelation distance

Fig. 10 Effect of vertical autocorrelation distance on the face ultimate support force

Figure 11 shows the effect of the cross correlation coefficient of the permeability coefficient on the face ultimate support force. It can be seen that as the cross correlation coefficient increases, the face ultimate support force increases. This is due to the fact that the positive correlation of the permeability coefficient makes the surrounding pore water more susceptible to the tunnel excavation, resulting in a greater seepage force. The dispersion of the calculated results is independent of the cross correlation coefficient. When the cross correlation coefficient is 0.1, the mean of the ultimate support force is 73.2 kPa; while the cross correlation coefficient is 0.8, the mean of the ultimate support force increases to 79.4 kPa, and the rate of increase is only 9%, the ultimate support force is slightly affected by the cross correlation coefficient of permeability coefficient.

6.4 Permeability coefficient ratio

Figure 12 illustrates the effect of the permeability coefficient ratio on the pore water pressure at the face, the calculated parameters are shown in case 4 in Table 3. It shows that when $k_y / k_x < 1$, the influence range of tunnelling on pore water pressure is large in the horizontal direction; when $k_y / k_x > 1$, the influence range is large in the vertical direction, and the vertical influence range gradually increases with the increase of the permeability coefficient ratio. The effect of the permeability coefficient ratio on the seepage velocity of the face is shown in Fig. 13. The seepage velocity at the face increases significantly with the increase of the permeability coefficient ratio, and accordingly, the seepage force component in the face support force significantly increases. It can be found by combining Figs.12 and 13 that the anisotropy of the permeability coefficient has a large influence on the calculated results of the pore water pressure field near the face.

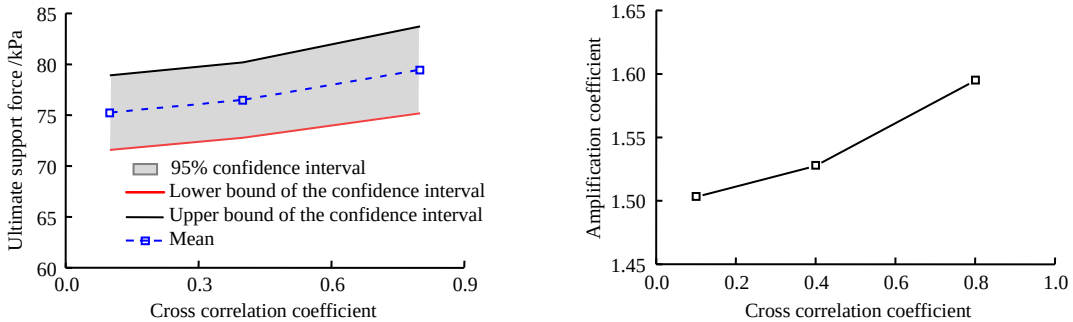

(a) Variation of ultimate support force with cross correlation coefficient

(b) Variation of amplification coefficient with cross correlation coefficient

Fig. 11 Effect of cross correlation coefficient on the face ultimate support force

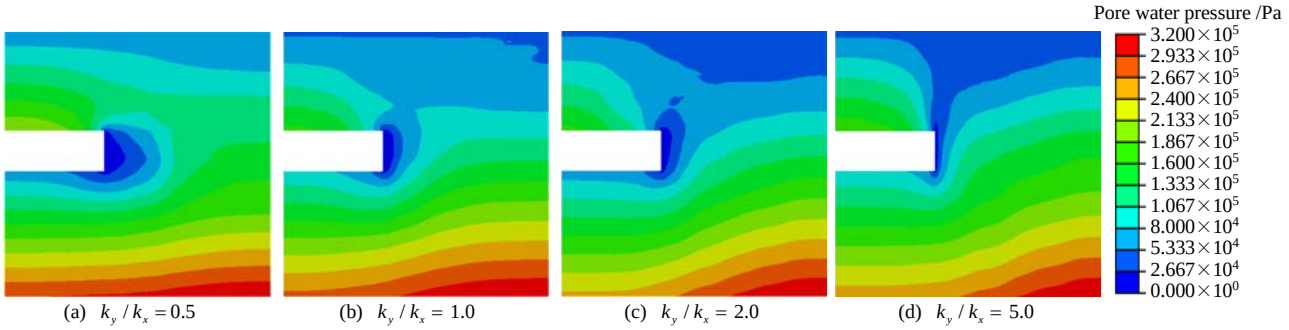

Fig. 12 Effect of permeability coefficient ratio on the face pore water pressure

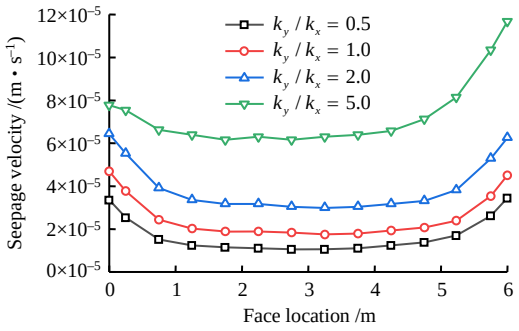

Fig. 13 Effect of permeability coefficient ratio on the face seepage velocity

The variation of the ultimate support force of the face with the anisotropy of the permeability coefficient is shown in Fig. 14. It can be seen from the figure that the ultimate support force increases significantly with the increase of the permeability coefficient ratio and the increase rate decreases gradually, which corresponds to the calculated results in Figs. 12 and 13 and is consistent with the calculated results provided in the literature[27]. However, the amplification coefficient of the ultimate support force tends to decrease linearly with the increase of the permeability coefficient ratio. This is due to the fact that the ultimate support force of the face increases with the increase of the permeability coefficient ratio under the condition of homogenous permeability coefficients.

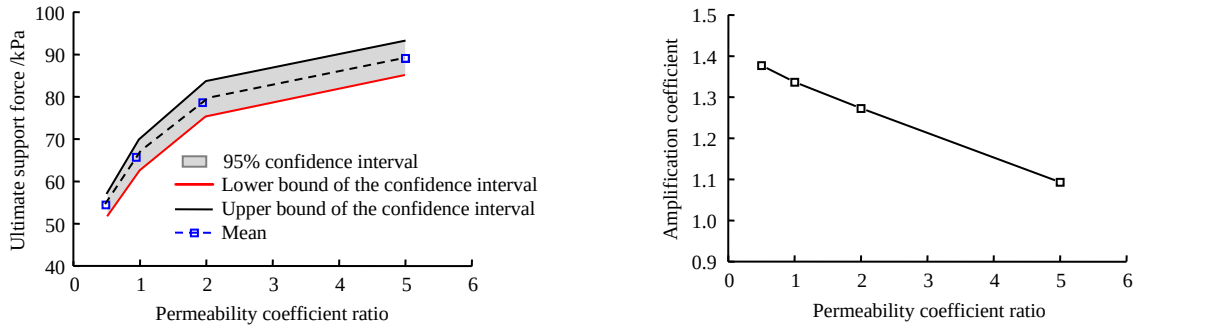

(a) Variation of ultimate support force with permeability coefficient ratio (b) Variation of amplification coefficient with permeability coefficient ratio

Fig. 14 Effect of permeability coefficient ratio on the face ultimate support force

7 Conclusion

(1) The spatial variability of the permeability coefficient increases the seepage force of the face and reduces the face stability. With the increase of the coefficient of variation of the permeability coefficient, the ultimate support force of the face gradually increases, and its dispersion and amplification coefficient also increase. The spatial variability of the permeability coefficient has less influence on the failure mechanism of the face. With the increase of the coefficient of variation, the failure range in the horizontal direction gradually decreases, and the failure range in the vertical direction gradually increases.

(2) As the horizontal autocorrelation distance increases, the amplification coefficient of the ultimate support force of the face gradually decreases; on the contrary, the amplification coefficient gradually increases with the increase of the vertical autocorrelation distance. The dispersion of the calculation result of the ultimate support force varies slightly with the autocorrelation distance.

(3) The increase of the ratio of vertical and horizontal permeability coefficients and its cross correlation coefficient can reduce the face stability, in which the influence of the permeability coefficient ratio is great but the influence of the cross correlation coefficient is small. The amplification coefficient of the ultimate support force exhibits a linearly decreasing trend with the increase of the permeability coefficient ratio.

References

[1] JANSSEN H A. Versuche uber getreidedruck in silszellen[J]. Zeitschr. d. Vereines deutscher Ingenieure, 1895, 39(35): 1045–1049.

[2] HORN N. Horizontal earth pressure on the vertical surfaces of the tunnel tubes[C]//Proceedings of the National Conference of the Hungarian Civil Engineering Industry. [S. l.]: [s. n.], 1961.

[3] LECA E, DORMIEUX L. Upper and lower bound solutions for the face stability of shallow circular tunnels in frictional material[J]. Géotechnique, 1990, 40(4): 581–606.

[4] SONG Chun-xia, HUANG Mao-song, LÜ Xi-lin. Upper bound analysis of plane strain tunnel in nonhomogeneous clays[J]. Rock and Soil Mechanics, 2011, 32(9): 2645–2650.

[5] LIANG Qiao, YANG Xiao-li, ZHANG Jia-hua, et al. Upper bound analysis for supporting pressure of shield tunnel in heterogeneous soil[J]. Rock and Soil Mechanics, 2016, 37(9): 2585–2592.

[6] LEE I M, NAM S W. The study of seepage forces acting on the tunnel lining and tunnel face in shallow tunnels[J]. Tunnelling and Underground Space Technology, 2001, 16(1): 31–40.

[7] HUANG Fu. Upper bound analysis of collapsing mechanism of surrounding rock and rockbolt supporting structures for tunnels[D]. Changsha: Central South University, 2012.

[8] MI Bo, XIANG Yan-yong. Model experiment and calculation analysis of excavation-seepage stability for shallow shield tunneling in sandy ground[J]. Rock and Soil Mechanics, 2020, 41(3): 837–848.

[9] GAO Jian, ZHANG Yi-tong, QIAO Jin-li. Face stability analysis of tunnels with consideration of seepage force[J]. Chinese Journal of Geotechnical Engineering, 2009, 31(10): 1547–1553.

[10] MOLLON G, DIAS D, SOUBRA A H. Probabilistic analysis of circular tunnels in homogeneous soil using response surface methodology[J]. Journal of Geotechnical and Geoenvironmental Engineering, 2009, 135(9): 1314–1325.

[11] LI Zhi-hua, HUA Yuan, ZHOU Tai-quan, et al. Research on reliability of excavation face stability in shield tunneling[J]. Rock and Soil Mechanics, 2008, 29(Suppl.1): 315–319.

[12] SUN Dao-guang. Reliability analysis for face stability of slurry shield tunnel[D]. Changsha: Central South University, 2014.

[13] MOLLON G, PHOON K K, DIAS D, et al. Validation of a new 2D failure mechanism for the stability analysis of a pressurized tunnel face in a spatially varying sand[J]. Journal of Engineering Mechanics, 2010, 137(1): 8–21.

[14] ESHRAGHI A, ZARE S. Face stability evaluation of a TBM-driven tunnel in heterogeneous soil using a probabilistic approach[J]. International Journal of Geomechanics, 2015, 15(6): 04014095.1-04014095.10.

[15] LÜ Jing, KE Xian-min, ZHANG xiao-xiao, et al. Variability of saturated permeability coefficient of loess slopes in South Jingyang tableland[J]. Bulletin of Soil and Water Conservation, 2017, 37(3): 254–257.

[16] PHOON K K, HUANG S P, QUEK S T. Implementation of Karhunen-loeve expansion for simulation using a wavelet-galerkin scheme[J]. Probabilistic Engineering Mechanics, 2002, 17(3): 293–303.

[17] LALOY E, ROGIERS B, VRUGT J A, et al. Efficient posterior exploration of a high-dimensional groundwater model from two-stage MCMC simulation and polynomial chaos expansion[J]. Water Resources Research, 2013, 49(5): 2664–2682.

[18] ZHANG J Z, HUANG H W, ZHANG D M, et al. Effect of ground surface surcharge on deformational performance of tunnel in spatially variable soil[J]. Computers and Geotechnics, 2021, 136: 1–14.

[19] ABID ALI, LYAMIN A V, HUANG J S, et al. Undrained stability of a single circular tunnel in spatially variable soil subjected to surcharge loading[J]. Computers and Geotechnics, 2017, 84: 16–27.

[20] NATAF. A determination des distributions de probabilites dont les marges sont donnees[J]. Comptes Rendus de l'Academie des Sciences, 1962, 225: 42–43.

[21] QIN Quan, LIN Dao-jin, MEI Gang. Theory and applications reliability stochastic finite element methods[M]. Beijing: Tsinghua University Press, 2006.

[22] LYAMIN A V, SLOAN S. Upper bound limit analysis using linear finite elements and non-linear pro-gramming[J]. International Journal for Numerical and Analytical Methods in Geomechanics, 2002, 26(2): 181–216.

[23] LYAMIN A V, SLOAN S W. Lower bound limit analysis using non-linear programming[J]. International Journal for Numerical Methods in Engineering, 2002, 55(5): 573–611.

[24] LEI Zhi-dong, YANG Shi-xiu, XU Zhi-rong, et al. Preliminary study on the spatial variability of soil properties[J]. Journal of Hydraulic Engineering, 1985(9): 12–23.

[25] MAKRODIMOPOULOS A, MARTIN C M. Upper bound limit analysis using simplex strain elements and second-order cone programming[J]. International Journal for Numerical and Analytical Methods in Geomechanics, 2007, 31(6): 835–865.

[26] LIU Quan-wei, YANG Zhong-nian. Model test research on excavation face stability of slurry balanced shield in permeable sand layers[J]. Rock and Soil Mechanics, 2014, 35(8): 2255–2260.

[27] LI Jun, CHEN Ren-peng, KONG Ling-gang. Model test study of the failure mechanism of shallow tunnels in dry sands[J]. China Civil Engineering Journal, 2011, 44(7): 142–148.

[28] ZHANG J Z, PHOON K K, ZHANG D M, et al. Novel approach to estimate vertical scale of fluctuation based on CPT data using convolutional neural networks[J]. Engineering Geology, 2021, 294: 1–10.

[29] JIANG Shui-hua, LI Dian-qing, ZHOU Chuang-bing, et al. Slope reliability analysis considering effect of autocorrelation functions[J]. Chinese Journal of Geo-technical Engineering, 2013, 36(3): 508–518.

[30] YUAN Shuai, FENG De-wang. Computational limit analysis of shield tunnel face with a consideration of permeability anisotropy[J]. Journal of Tongji University (Natural Science), 2020, 48(12): 1717–1725.